Rovibrational quantum interferometers and gravitational waves

Andreas Wicht*
Institut für Experimentalphysik, Heinrich-Heine-Universität Düsseldorf, Universitätsstraße 1, 40225 Düsseldorf, Germany

Claus Lämmerzahl, Dennis Lorek, and Hansjörg Dittus
Center of Applied Space Technology and Microgravity, Am Fallturm, D-28359 Bremen, Germany
(Received 8 October 2007; revised manuscript received 16 April 2008; published 7 July 2008)

We show that the application of atom interferometry techniques to the internal, i.e., rotational-vibrational states of molecules provides a new tool for ultrahigh precision tests of fundamental physics. The measurement principle is based on the fact that the electronic structure of molecules is not spherically symmetric. A diatomic quantum sensor can hence distinguish between the direction along its internuclear axis and the two orthogonal directions and is therefore direction sensitive. As an example we show how a molecular rotational-vibrational quantum interferometer based on the hydrogen deuteride molecular ion (HD^+) may be used to detect gravitational waves. We show that a monochromatic gravitational wave of dimensionless amplitude $h=10^{-19}$ will cause a frequency shift of the order of 30 μHz between appropriately prepared quantum states, a frequency difference likely to be detectable with the next generation atom interferometers in 1 s.

DOI: 10.1103/PhysRevA.78.013610 PACS number(s): 03.75.Dg, 04.80.Nn, 33.80.−b, 37.25.+k

I. INTRODUCTION

Thanks to the recent progress in the fields of optical metrology [1] and cold molecules [2] a new tool for precision measurements, especially for precision tests of fundamental physics, has come into reach. While optical frequency combs now provide the means to generate, at arbitrary frequency, optical fields that are phase stable with respect to an ultrastable radio frequency (rf) or an optical reference oscillator, molecular physics is about to solve the problem of how to create translationally cold molecules that are also internally cold. With these tools at hand, coherent manipulation of individual internal molecular states now seems feasible and, hence, should open new perspectives for quantum computation with molecules [3], quantum state selective chemistry [4], or even for the implementation of matter wave interferometers. The latter would then rely on the coherent manipulation of different individual rotational-vibrational molecular quantum states and should therefore be considered a rovibrational quantum interferometer.

In contrast to the electronic structure of atoms, the electronic structure of molecules is not spherically symmetric. Diatomic molecules can distinguish between different directions in space as defined relative to the direction of their internuclear axis. This makes them perfect probes for experiments that aim at the investigation of anisotropic effects, such as tests of the isotropy of the Coulomb force [5] or tests of the standard model extension [6]. In this paper we demonstrate that rovibrational quantum interferometers could even provide the basis for an atomic scale gravitational wave detector. As we will point out, quantum-physical probes show a number of unique features, that in a twofold sense "classical" gravitational wave detectors, such as laser interferometers [7] or bar-type detectors [8], are missing.

It should be pointed out that molecule-based matter wave interferometers have already been implemented. However, these were based on interference between quantum states describing the translational and the electronic [9], or the hyperfine [10] rather than the rovibrational degrees of freedom and as such resemble atom interferometers. Further, ultrashort (fs) laser pulses have been used to create and investigate coherence between a large number of rovibrational states [11]. However, due to their broad spectral width, fs laser pulses do not provide coherent control over individual rovibrational states. Thus, they are not suited for the implementation of precision rovibrational quantum interferometers.

This paper starts out by showing in Sec. II why atom interferometry [12] is the most sensitive laboratory measurement tool in science. We refer to an example, the Stanford atom interferometer for the determination of the fine-structure constant [13], in order to outline the basic idea of how a quantum interferometer can provide a test of fundamental physics with ultrahigh sensitivity. The Stanford experiment also provides an estimate for the sensitivity that rovibrational quantum interferometers could in principle reach with existing technology. Section III then describes qualitatively how to implement a gravitational wave detector (and any other type of direction sensitive quantum detector) on the basis of a rovibrational quantum interferometer. In the subsequent section, Sec. IV, we derive the Hamiltonian for a charged point mass (e.g., the electron) in the field of another point charge (the proton or deuteron) taking into account the presence of a gravitational wave. The result provides the means to construct the perturbation operator that describes the modification of the HD^+ (ion of the molecule hydrogen deuteride) molecular Hamiltonian by the gravitational wave. This is done in Sec. V. In Sec. VI the perturbation operator is evaluated, the optimal rovibrational quantum interferometer is constructed, and its sensitivity to gravitational waves is estimated. We are then prepared to compare rovibrational quantum interferometric gravitational wave detectors to classical laser interferometric and bar-type detectors as well as to atom interferometric detectors in Sec. VII.

Let us emphasize that the application of rovibrational quantum interferometers to gravitational wave detection just

*andreas.wicht@gmx.net

serves as an example for molecular quantum interferometry. The main purpose of this paper is to convince the reader that quantum interferometers based on the coherence between individual rotational-vibrational states hold promise for becoming a powerful tool for ultrahigh precision spectroscopy.

II. ATOM INTERFEROMETRY

Atom interferometry [12] has become the most accurate and sensitive laboratory measurement tool in science. Applications include, for example, the determination of the fine-structure constant [13], of the gravitational acceleration [14], and of gravity gradients [15]. Atom interferometers can also be used as inertial sensors [16], as they have been proposed for experiments aiming at a test of general relativity [17], and they have even been considered for gravitational wave detection [18]. Atom interferometers owe their prominent role to three unique features. First, an atom interferometry experiment can be considered a frequency measurement and hence, atom interferometry is linked to the most accurately implemented fundamental SI unit, the second. Second, atom interferometers are actually phase (rather than frequency) sensitive devices, which is another ingredient to the impressive accuracy they can deliver in a frequency measurement. Finally, atom interferometers provide a truly differential phase (and frequency) measurement: An atom interferometer measures the differential phase evolution between the two quantum states associated with the two paths of the interferometer.

Another point so far has not been appreciated enough. For certain applications, a "lever arm" can be implemented to boost the sensitivity of an atom interferometer. Then atom interferometry can surpass the sensitivity and accuracy of regular ultrahigh resolution laser spectroscopy by orders of magnitude. As an example we consider the Stanford atom interferometer for the determination of the fine-structure constant [13]. It actually constitutes a very precise measurement of the recoil splitting of an atomic resonance line, which results from the fact that an atom of finite mass acquires or releases kinetic energy when absorbing or emitting a photon. For the cesium $D1$ line this splitting amounts to 3.75 kHz. A regular laser spectroscopy experiment would determine the frequencies of the two doublet components individually. The ultimate precision and accuracy would then be limited by the precision and accuracy of the laser frequency. Phase locking ultrastable lasers to a cesium clock or to an optical clock will currently (at most) provide an absolute accuracy and precision of 0.1…1 Hz. Hence regular laser spectroscopy [19] would be able to deliver the recoil splitting with an accuracy and precision of 1 part in 10^4. In contrast, the Stanford atom interferometer has determined the recoil splitting with an uncertainty of 15 parts in 10^9, surpassing regular laser spectroscopy by four orders of magnitude. This accuracy corresponds to a relative shift of the cesium $D1$ transition frequency of 1 part in 10^{19}!

This remarkable sensitivity relies on a "lever arm" build into the photon-recoil atom interferometer. The principle of this "lever arm" is explained with the help of Fig. 1. The two states $|1\rangle$ and $|2\rangle$ denote the quantum states corresponding to

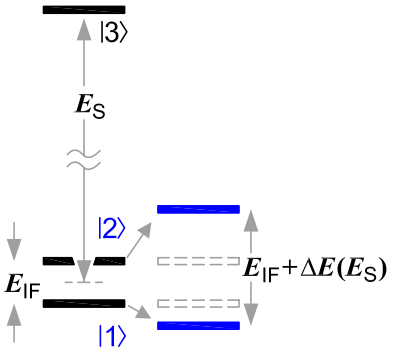

FIG. 1. (Color online) Atom interferometric differential measurement principle. The atom interferometer is constructed from states $|1\rangle$ and $|2\rangle$. It determines the energy difference between these two almost degenerate states through a differential phase measurement which yields, in principle, $\phi = E_{IF}/\hbar t$. The effect under study causes a differential energy shift $\Delta E = hE_S$ between the interferometer states that scales with some optical frequency E_S rather than with the small energy difference E_{IF}.

the two paths of the atom interferometer. The interferometer is constructed in such a way, that the effect under study shifts the energy of the two states by a differential amount $\Delta E = f(E_S)$ that does not scale with the small energy difference E_{IF} between the interferometer states but rather with the energy of an optical transition E_S, e.g., with the ionization energy of an atom. The absolute accuracy and sensitivity of the atom interferometric phase measurement are then ultimately limited by the accuracy and stability of the local oscillator bridging the energy difference E_{IF}. The frequency of that local oscillator can be locked to a highly stable reference oscillator with relative stability or accuracy ϵ_{ref}. This could be an atomic or optical clock, so that at best $\epsilon_{ref} \sim 10^{-15}$. The atom interferometer will therefore not be more accurate and precise than $\delta E_{min} = \epsilon_{ref} E_{IF}$. Let us assume, that the effect under study causes a shift of $\Delta E = hE_S$. The minimum detectable h will then be given by

$$h_{min} = \epsilon_{ref}\left(\frac{E_{IF}}{E_S}\right). \tag{1}$$

While the sensitivity of atom interferometry relies on the stability of the local oscillator bridging the small energy difference E_{IF}, regular laser spectroscopy needs to bridge an optical energy difference E_S. Accordingly, regular laser spectroscopy will resolve a minimum h of $h_{min} = \epsilon_{ref}$. Hence, the atom interferometer enhances the sensitivity by a factor of E_S/E_{IF}, which we refer to as "the lever arm." For the photon recoil experiment this lever arm amounts to 8.9×10^{10} and to 36×10^3 with respect to accuracy and noise, respectively [20].

The sensitivity of the photon-recoil experiment [13] was limited by the phase noise of the optical fields which were used to construct the atom interferometer. The experiment is currently being rebuilt to improve the sensitivity and to reduce systematic effects even further. For example, the new laser source provides a stability that is sufficient to measure a shift hE_S of an optical frequency with a sensitivity of

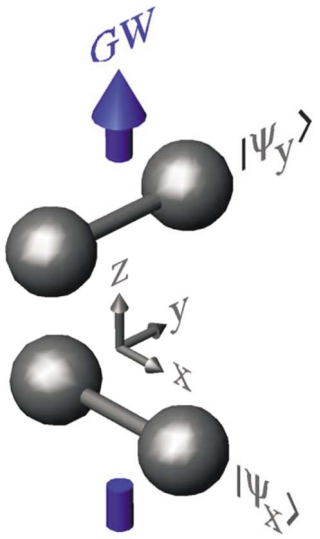

FIG. 2. (Color online) Molecular rovibrational quantum interferometer for the detection of gravitational waves. A molecule is prepared in a superposition of two orientational states, $|\psi_x\rangle$ and $|\psi_y\rangle$, which correspond to an alignment of the internuclear axis along the x and y direction and which denote the two paths of a quantum interferometer. The gravitational wave is propagating along the z direction. Due to the interaction with the gravitational wave a quantum phase shift will accumulate between these two states, which is read out by means of quantum interferometric methods.

20 μHz in 1 s corresponding to less than 1 part in 10^{19} in 1 s [21]. More likely, the sensitivity will be limited to 160 μHz in 1 s due to atom number shot noise [22]. An increase of the total atom number from 10^6 to 10^8 is well feasible with advanced laser cooling techniques and would bring the sensitivity level down to 20 μHz in 1 s. This demonstrates that state-of-the-art atom interferometer techniques are about to reach a sensitivity level of $h_{\min}=10^{-19}$ in 1 s.

III. MOLECULAR INTERFEROMETRY: QUALITATIVE DESCRIPTION

We will now transfer the concept of atom interferometry to molecules. To this end we will make use of a rather intuitive and incomplete description in this section in order to convey the basic ideas underlying rovibrational quantum interferometry. A detailed description then follows in the subsequent sections.

The basic idea is shown in Fig. 2. We prepare a sample of diatomic molecules in an appropriate (rovibrational) quantum state. We then apply a multichromatic laser pulse which coherently transfers the molecules from this initial state to a superposition $|\psi_x\rangle$ of rotational states such that maximal alignment of the internuclear axis along the x axis is achieved. A different laser pulse creates an alignment $|\psi_y\rangle$ along the y axis.

Let us now assume that a monochromatic gravitational wave (GW) [23] of angular frequency Ω_{GW} is propagating along the z direction, and that in transverse traceless (TT) gauge its polarization and instantaneous strain are given by $h_{xx}=-h_{yy}=h\cos(\Omega_{\mathrm{GW}}t)$. If we consider the two nuclei to be free-falling test masses for a moment, then it is obvious that the quadrupole nature of the GW will modify the internuclear distance related to the two orientational states $|\psi_x\rangle$ and $|\psi_y\rangle$ in a differential way: For example, it will increase the internuclear distance along the x axis and it will decrease it along the y axis. However, the nuclei are not free-falling but are bound to each other by the Coulomb interaction between all charged particles. The nuclei are hence no longer at internuclear equilibrium distance and will therefore readjust. Thus, it is expected that the GW modifies the rovibrational motion of the molecules differently for the two orientational quantum states. We can now add quantum interferometry to perform a truly differential measurement by preparing the molecules in a coherent superposition of states $|\psi_x\rangle$ and $|\psi_y\rangle$ rather than in just one of these states. The differential nature of GW interaction imprints a differential phase shift onto the two orientational quantum states which can then be read out by quantum (atom) interferometry techniques.

The two orientational interferometer states could either be degenerate ($E_{\mathrm{IF}}=0$) or the energy difference could be of the order of the rovibrational energy. As we will show later, the energy shift of the orientational states induced by the GW is of the order of $\Delta E=0.1hR_\infty$, where $R_\infty=m_e e^4/(32\pi^2\hbar^2\epsilon_0^2)$ is the Rydberg energy. Hence, the energy shift scales with an optical frequency while the two interferometer states are nearly degenerate. It is therefore possible to implement the "lever arm" discussed in Sec. II.

Gravitational waves generated by massive astrophysical objects cover the spectrum from a few kHz down to the μHz range. In any case, the GW frequency will be small compared to rotational, vibrational, or even electronic frequencies of molecules. The molecules will therefore adiabatically follow the action of the GW, so that the perturbation can be considered static. However, GWs are indeed time dependent. For a periodic gravitational wave the phase shift accrued between the two orientational states will be reversed after one-half of a GW period, so that the phase shift vanishes when averaged over a full period. This is known as the storage time limit in the field of laser interferometric gravitational wave detectors. Quantum interferometers offer an easy way to overcome this limitation: After one-half of a gravitational wave period we apply a laser pulse which coherently converts $|\psi_x\rangle$ into $|\psi_y\rangle$ and vice versa. This would correspond to swapping the light between the two arms of a laser interferometric GW detector. We can then continue to integrate the signal coherently and do not need to read out the phase shift after one-half of a gravitational wave period.

We next describe how a (rovibrational) quantum interferometer is optimized for a given application. Once a molecular sample is prepared in an appropriate quantum state, multichromatic laser pulses are used to coherently "inject" or transfer the population into the two paths of the quantum interferometer. The exact definition of the quantum states that correspond to these two paths depends on the specific application one has in mind. For a given application these quantum states are optimized by diagonalization of the complete Hamiltonian and subsequent analysis of the eigenvalues and eigenstates. Let us assume that the perturbation to the molecular Hamiltonian $\hat{\mathcal{H}}_0$ can be described by the op-

erator $\delta\hat{\mathcal{H}}=h(t)\delta\hat{H}$, where $h(t)$ denotes the slowly varying "strength" of the perturbation and $\delta\hat{H}$ is constant. The eigenvalues E_i corresponding to the eigenstates $|i\rangle$ of the full problem can then be written as $E_i=E_i^{(0)}+c_ih$ where the $E_i^{(0)}$ denote the energies of the eigenstates in the limit of vanishing perturbation and the c_ih give the perturbation energies. Let us from hereon omit the explicit time dependence of $h(t)$. We now pick two of these eigenstates, $|\psi_i\rangle$ and $|\psi_j\rangle$, to define the two paths of the interferometer. The energy difference between these states is given by $\Delta_{ij}=(c_i-c_j)h+\Delta E_{ij}$, where $\Delta E_{ij}=E_i^{(0)}-E_j^{(0)}$. Thus, a phase difference of $\Delta\phi_{ij}=(1/\hbar)[(c_i-c_j)h+\Delta E_{ij}]t$ will accrue between these states with time. The quantum interferometer is constructed in such a way that the contribution from ΔE_{ij} is eliminated by the interaction with the multichromatic laser pulses. However, this cancellation relies on the accuracy and stability of the local oscillator used to define the (relative) phase of all laser fields. Any phase error of the local oscillator could show up as a contribution to the phase difference and would then eventually mask the signal. The optimization of the two quantum paths therefore is led by finding a pair of states with large (c_i-c_j) but sufficiently small ΔE_{ij}, so that the lever arm of Sec. II can become effective.

It should be noted that the optimization of the interferometric quantum states described above constitutes a generalization of the existing quantum interferometry concept.

With the basic idea of molecular interferometry in mind we are now prepared for a more detailed discussion.

IV. GRAVITATIONAL WAVES AND CHARGED POINT MASSES

Gravitational waves are small perturbations in a background space-time metric and, thus, can be described within linearized gravity. With a flat Minkowski background metric $\eta_{\mu\nu}=\mathrm{diag}(-1,1,1,1)$, the metric $g_{\mu\nu}$ is then written as

$$g_{\mu\nu}=\eta_{\mu\nu}+h_{\mu\nu},\quad |h_{\mu\nu}|\ll 1. \tag{2}$$

For simplicity, we choose a coordinate system so that the perturbations are transverse and traceless (TT gauge) and obey in vacuum [23,24]

$$\Box h_{ij}^{\mathrm{TT}}=0,\quad h_{\mu 0}^{\mathrm{TT}}=0,\quad \delta^{kl}h_{ik,l}^{\mathrm{TT}}=0,\quad \delta^{ij}h_{ij}^{\mathrm{TT}}=0, \tag{3}$$

where $\Box$ is the d'Alembertian operator based on the Minkowski metric and commas denote partial derivatives (in the following the superscript TT will be omitted as we are always in TT gauge). As a consequence, gravitational waves have helicity ± 2 and only spatial components h_{ij} orthogonal to the direction of propagation are nonzero. For instance, plane waves propagating along the x^3 axis are given by only two independent components of the amplitude h_{ij} (two polarizations h_+, $h_\times$),

$$\begin{aligned} h_{11}(x)&=-h_{22}(x)=h_+(t-z/c),\\ h_{12}(x)&=h_{21}(x)=h_\times(t-z/c),\\ h_{0\mu}(x)&=h_{\mu 0}(x)=h_{\mu 3}=h_{3\mu}=0, \end{aligned} \tag{4}$$

where $ct=x^0$ and $z=x^3$. In the TT gauge the pertinent components of the Riemann curvature tensor have the simple form

$$R_{i0j0}=-\frac{1}{2}h_{ij,00} \tag{5}$$

and are gauge invariant to linear terms in $h_{\mu\nu}$ [23,25].

Now, we analyze how gravitational waves modify the Hamiltonian of a charged point mass (e.g., an electron) in the field of another point charge (here, proton or deuteron). We start with the Klein-Gordon equation minimally coupled to gravity and to the Maxwell field

$$g^{\mu\nu}D_\mu D_\nu\psi-\frac{m^2c^2}{\hbar^2}\psi=0. \tag{6}$$

The covariant derivative D_μ is given by

$$D_\mu T^\nu=\partial_\mu T^\nu+\left\{\begin{matrix}\nu\\ \mu\sigma\end{matrix}\right\}T^\sigma-\frac{ie}{\hbar c}A_\mu T^\nu, \tag{7}$$

where the braces denote the Christoffel symbol

$$\left\{\begin{matrix}\nu\\ \mu\sigma\end{matrix}\right\}:=\frac{1}{2}g^{\nu\rho}(\partial_\mu g_{\sigma\rho}+\partial_\sigma g_{\mu\rho}-\partial_\rho g_{\mu\sigma}) \tag{8}$$

and A_μ is the Maxwell potential. We insert the above metric (2) into (6) and make for the wave function ψ the ansatz [26]

$$\psi=\exp\left(\frac{i}{\hbar}(c^2S_0+S_1+c^{-2}S_2+\cdots)\right), \tag{9}$$

which is also inserted into (6). We compare equal powers of the expansion parameter c^2 where $(e/c)A_i$ is treated to be of order 1 (terms of this kind must appear in the nonrelativistic Schrödinger equation) [27]. Here, we also made use of the Lorenz gauge $g^{\mu\nu}D_\mu A_\nu=0$, the TT gauge (3), and we neglected terms quadratic in $h_{\mu\nu}$.

The lowest-order equation implies that S_0 is a function of time only. The next order gives the solution $S_0=-mt$. The substitution $\tilde{\phi}:=\exp[(i/\hbar)S_1]$ then transforms the next-order equation to a Schrödinger equation for $\tilde{\phi}$,

$$i\hbar\partial_t\tilde{\phi}=\mathcal{H}\tilde{\phi}, \tag{10}$$

where the Hamiltonian is given by (see also [28])

$$\mathcal{H}=-\frac{\hbar^2}{2m}(\delta^{ij}-h^{ij})\partial_i\partial_j-eA_0+\frac{ie\hbar}{m}\frac{A_i}{c}(\delta^{ij}-h^{ij})\partial_j. \tag{11}$$

Since for nonrelativistic systems magnetic fields are much smaller than electric fields they can be neglected. The interaction part of the above Hamiltonian is therefore given by

$$\mathcal{H}_1=\frac{\hbar^2}{2m}h^{ij}\partial_i\partial_j. \tag{12}$$

The next step is to analyze how the electric potential A_0 of a point charge q is modified by the presence of a gravitational wave. We use the inhomogeneous Maxwell equations coupled to gravity

$$4\pi j^{\mu} = D_{\nu}(g^{\mu\rho}g^{\nu\sigma}F_{\rho\sigma}), \tag{13}$$

where $F_{\rho\sigma}=\partial_{\rho}A_{\sigma}-\partial_{\sigma}A_{\rho}$. Inserting again the metric (2) into (13) and considering a point charge $[j_0=q\delta^3(r)$ and $j_i=0]$, we obtain

$$-4\pi q\delta^3(r) = \Box A_0 - h^{ij}\partial_i\partial_j A_0 + \frac{i\omega}{c}h^{ij}\partial_i A_j, \tag{14}$$

$$0 = \Box A_i - h^{jk}\partial_j\partial_k A_i + \frac{i\omega}{c}h_i^j\partial_j A_0. \tag{15}$$

Here, we took the Lorenz and TT gauge (3) into account and specified $h_{\mu\nu}$ for the case of periodic gravitational waves $h_{\mu\nu}=h^0_{\mu\nu}\exp[i(\vec{k}\vec{x}-\omega t)]$ with amplitudes $h^0_{\mu\nu}$. If one now makes the assumption that the influence of a gravitational wave is adiabatic (small frequency) and quasiconstant (long wavelength), then the factor $\exp[i(\vec{k}\vec{x}-\omega t)]$ is nearly constant over the dimension of a molecule. In this case, the potentials can be considered static and (14) and (15) can be solved with the help of the ansatz $A_0=q/r+qA_0^{(1)}$, $A_i=qA_i^{(1)}$, where $A_{\mu}^{(1)}$ denotes the first-order correction in $h^0_{\mu\nu}$. To first order we finally obtain the potentials A_{μ} of a point charge q in the field of a gravitational wave,

$$A_0 = \frac{q}{r}\left(1 - \frac{x^i h^0_{ij} x^j}{2r^2}e^{i(\vec{k}\vec{x}-\omega t)}\right), \tag{16}$$

$$A_i = -q\frac{h^0_{ij}x^j}{r^2}e^{i(\vec{k}\vec{x}-\omega t)}. \tag{17}$$

While this specific form of the above results (12) and (16) depends on the chosen TT gauge condition the observed energy should not. In fact, for atom interferometry [18] and for the calculation of the cross section of the absorption of gravitational waves by atomic systems [28], it has been shown that identical results can be obtained in Fermi normal coordinates. The same holds in our case.

V. GRAVITATIONAL WAVES AND THE HD^+ MOLECULE

In this section the perturbation of the molecular Hamiltonian due to a gravitational wave will be derived. For the sake of simplicity we will consider the H_2^+ molecule and its isotopomers, specifically the HD^+ molecule.

The total molecular Hamiltonian is given by $\hat{\mathcal{H}}=\hat{\mathcal{H}}_0+\delta\hat{\mathcal{H}}$, where $\hat{\mathcal{H}}_0$ describes the unperturbed part and $\delta\hat{\mathcal{H}}$ denotes the perturbation due to the interaction with the gravitational wave. Let us first restrict the discussion to the unperturbed situation in order to point out the approximations we apply in the subsequent discussion. The unperturbed Hamiltonian is given by

$$\hat{\mathcal{H}}_0 = \hat{T}_e + \hat{V}_{en} + \hat{T}_n + \hat{V}_{nn}, \tag{18}$$

the contributions of which will be defined in the following. Let $|\Psi\rangle=|\vec{x}\rangle|\vec{x}_{(1)}\rangle|\vec{x}_{(2)}\rangle$ define a set of basis states where $\vec{x}$, $\vec{x}_{(1)}$, and $\vec{x}_{(2)}$ denote the position of the electron, of nucleus 1, and of nucleus 2, respectively. The kinetic energy of the electron is then given by $\hat{T}_e=\int d\Psi T_e|\Psi\rangle\langle\Psi|$ with

$$T_e = -\frac{\hbar^2}{2m_e}\sum_{i=1}^{3}\partial_i\partial_i. \tag{19}$$

Similarly, the kinetic energy of the two nuclei is given by $\hat{T}_n=\int d\Psi T_n|\Psi\rangle\langle\Psi|$ with

$$T_n = -\sum_{i=1}^{3}\left(\frac{\hbar^2}{2m_1}\partial_{(1)\,i}\partial_{(1)\,i} + \frac{\hbar^2}{2m_2}\partial_{(2)\,i}\partial_{(2)\,i}\right), \tag{20}$$

and the electron-nuclei Coulomb interaction is $\hat{V}_{en}=\int d\Psi V_{en}|\Psi\rangle\langle\Psi|$ with

$$V_{en} = \frac{1}{4\pi\epsilon_0}\left\{\frac{q_e q_1}{|\vec{x}-\vec{x}_{(1)}|} + \frac{q_e q_2}{|\vec{x}-\vec{x}_{(2)}|}\right\}. \tag{21}$$

Finally $\hat{V}_{nn}=\int d\Psi V_{nn}|\Psi\rangle\langle\Psi|$ gives the nuclear Coulomb interaction where

$$V_{nn} = \frac{1}{4\pi\epsilon_0}\frac{q_1 q_2}{|\vec{x}_{(1)}-\vec{x}_{(2)}|}. \tag{22}$$

To separate the nuclear center-of-mass motion in (18) we introduce the nuclear center-of-mass (c.m.) coordinate $\vec{R}_{\text{c.m.}}=(m_1\vec{x}_{(1)}+m_2\vec{x}_{(2)})/M$, where M is the total nuclear mass. Further, $\vec{R}=\vec{x}_{(2)}-\vec{x}_{(1)}$ denotes the internuclear distance vector. With these definitions $|\Psi\rangle\langle\Psi|$ becomes $|\Psi\rangle\langle\Psi|=|\vec{x}\rangle|\vec{R}\rangle|\vec{R}_{\text{c.m.}}\rangle\langle\vec{R}_{\text{c.m.}}|\langle\vec{R}|\langle\vec{x}|$. Including the perturbation by the GW for a moment we find, that the kinetic energy $T_n^M=-\hbar^2/(2M)\Sigma_i\partial_{R_{\text{c.m.},i}}\partial_{R_{\text{c.m.},i}}$ associated with the motion of the total nuclear mass is modified according to (12). However, this modification is not specific to molecules and will therefore not be considered any further. We can hence replace the nuclear kinetic energy $\hat{T}_n$ in (18) by the kinetic energy associated with the motion of the reduced nuclear mass $m=m_1m_2/(m_1+m_2)$, that is by $\hat{T}_n^m=\int d\Psi T_n^m|\Psi\rangle\langle\Psi|$ with

$$T_n^m = -\frac{\hbar^2}{2m}\sum_{i=1}^{3}\partial_{R_i}\partial_{R_i}. \tag{23}$$

We restrict the discussion to the molecular electronic ground state. An approximation to the corresponding electronic part of the molecular wave functions is constructed with the Heitler-London approach [29], i.e., by a superposition of two atomic hydrogen ground-state wave functions $|1\rangle$ and $|2\rangle$ that describe an electron orbiting around nuclei 1 and 2, respectively:

$$|\pm\rangle = C_{\pm}(|1\rangle \pm |2\rangle). \tag{24}$$

The atomic wave functions $|i\rangle$ are [29]

$$\langle\vec{x}|i\rangle = \psi_i(\vec{x}) = (\pi a^3)^{-1/2}\exp\left(-\frac{|\vec{x}-\vec{x}_{(i)}|}{a}\right), \tag{25}$$

where $a=4\pi\epsilon_0\hbar^2/(m_e e^2)$ is the Bohr radius. Further, $C_{\pm}$ is the normalization constant [29]

$$C_{\pm} = \left[2 + 2\left(1 + \frac{R}{a} + \frac{R^2}{3a^2} \right) \exp\left(-\frac{R}{a} \right) \right]^{-1} \tag{26}$$

with $R = |\vec{R}|$ denoting the internuclear distance. The antisymmetric linear combination $|-\rangle$ corresponds to an antibinding molecular state and will therefore not be considered any further.

We now apply the Born-Oppenheimer approximation to derive the effective Hamiltonian associated with the relative nuclear motion. To this end we evaluate the expectation value of the unperturbed Hamiltonian with respect to the electronic coordinate for the Heitler-London molecular wave function $|+\rangle$ defined in (24), i.e., we determine $\hat{V}_{\mathrm{BO}} = \langle + | \hat{H}_0 | + \rangle$. The effective Hamiltonian that approximately describes the relative nuclear motion then reads $\hat{V}_{\mathrm{BO}} = \int d^3R\, V_{\mathrm{BO}} |\vec{R}\rangle\langle\vec{R}|$ with

$$V_{\mathrm{BO}} = T_n^m + V_{nn} + \int d^3x \langle + | x \rangle (T_e + V_{en}) \langle x | + \rangle. \tag{27}$$

We finally switch from Cartesian to spherical coordinates for the internuclear distance vector $\vec{R}$ and rewrite the Hamiltonian accordingly.

We could now solve the Schrödinger equation for the motion of the reduced mass as defined by the effective Born-Oppenheimer Hamiltonian (27). However, we would then encounter two difficulties. First, we would have to solve for a radial motion in an anharmonic potential. As long as low-lying vibrational states are considered the anharmonicity would create only a small correction to a description based on a harmonic approximation, but it would nevertheless severely increase the efforts necessary to numerically determine the perturbation operator. We have therefore decided to approximate the effective Hamiltonian by a harmonic potential. Second, the rotational motion adds a centrifugal barrier to the radial motion so that for each rotational quantum number l, a different effective potential and consequently different vibrational wave functions would have to be calculated. Again, for low-lying rotational states this would give rise to only a small correction to a model that ignores coupling between the rotational and the vibrational motion (mostly the centrifugal force). However, inclusion of the coupling would severely increase the efforts necessary to determine the perturbation operator. We have therefore decided to ignore the coupling. We rather use the approximate harmonic potential and solve the radial motion for the case of the rotational ground state. These vibrational states are then considered to also describe the radial motion for higher rotational quantum states adequately.

Within the framework of these approximations the rovibrational eigenstates with vibrational quantum number v, rotational quantum number l and magnetic quantum number m can easily be calculated. We omit this step here and refer to the literature for details, e.g., [29]. The rovibrational eigenstates within the bound molecular electronic ground state are then given by

$$|\psi_{vlm}\rangle = C_+ (|1\rangle + |2\rangle) |v\rangle |lm\rangle, \tag{28}$$

where in spherical coordinates

$$\langle \vec{R} | v \rangle | lm \rangle = \left\{ \frac{1}{R} u_v \left(\frac{R - R_0}{R_{00}} \right) \right\} Y_{lm}(\theta, \phi).$$

The $Y_{lm}(\theta, \phi)$ denote the spherical harmonics [30], and

$$u_v(\kappa) = \sqrt{\frac{1}{2^v v!\sqrt{\pi} R_{00}}} H_v(\kappa) \exp\left(-\frac{1}{2}\kappa^2 \right) \tag{29}$$

describes the radial dependence of the wave function. Here, $H_v(\kappa)$ are the Hermite polynomials [30], and R_0 and R_{00} denote the internuclear equilibrium distance and the vibrational amplitude for the rotational ground state, respectively. The vibrational amplitude is determined by the reduced nuclear mass m and the vibrational frequency ω_{00} through $R_{00} = [\hbar/(m\omega_{00})]^{(1/2)}$ [29]. Within the Heitler-London approach the corresponding values are $R_0 = 2.492\,83\,a$ for H_2^+ and HD^+, and $R_{00} = 0.362\,857\,a$ for H_2^+ and $R_{00} = 0.256\,579\,a$ for HD^+.

We are now prepared to calculate the perturbation Hamiltonian in the basis of the unperturbed eigenstates. We first transform into the interaction picture, which eliminates the unperturbed Hamiltonian from the Schrödinger equation. We then recognize that GWs in the μHz to kHz range cannot drive transitions between rovibrational states that differ with respect to the vibrational or rotational quantum number, because the corresponding transition frequencies are in the THz range. We then apply the rotating-wave approximation and conclude that the perturbation operator will effectively have nonzero matrix elements only between rovibrational states that correspond to the same electronic, vibrational, and rotational quantum number, i.e.,

$$\langle v | \langle lm | \delta\hat{H} | l'm' \rangle | v' \rangle \sim \delta_{vv'} \delta_{ll'}. \tag{30}$$

Next, let us assume that a gravitational wave is propagating along the z axis with a polarization (in TT gauge) defined by

$$h_{xx} = -h_{yy} = h_+ = h \cos \Omega_{\mathrm{GW}} t, \quad h_{zz} = 0. \tag{31}$$

Each of the contributions to the unperturbed Hamiltonian in (18) will be modified by the presence of the gravitational wave and will give rise to a perturbation according to (12) or (16). According to (12) the perturbation to the electronic kinetic energy is then given by

$$\delta T_e = h \frac{\hbar^2}{2m_e} (\partial_1^2 - \partial_2^2). \tag{32}$$

Within the framework of the Born-Oppenheimer approximation (27) numerical integration of this perturbation over the electronic coordinate delivers the following contribution to the effective potential, given in spherical coordinates:

$$\delta T_{e,\mathrm{BO}} = \int d^3x \langle + | x \rangle \delta T_e \langle x | + \rangle$$

$$= (hR_\infty)\, \delta\tilde{T}_e(\rho) \cos(2\phi) [1 - \cos(2\theta)], \tag{33}$$

where

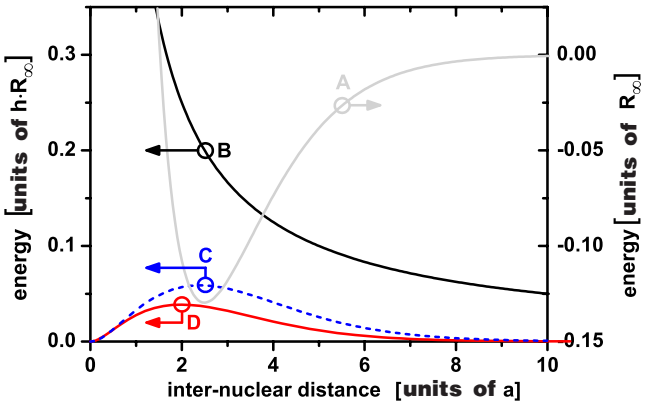

FIG. 3. (Color online) Effective potential and perturbations for the H_2^+ and HD^+ molecule based on a Heitler-London approach for the electronic molecular wave function. *A* shows the unperturbed potential V_{BO} according to (27) [29]. *B*, *C*, and *D* show the radial dependence of the perturbation to the nuclear Coulomb energy, $\delta\tilde{V}_{nn}(\rho)$ (38), to the electronic kinetic energy, $\delta\tilde{T}_e(\rho)$ (33), and to the electronic Coulomb energy, $\delta\tilde{V}_{en}(\rho)$ (36), respectively. The internuclear distance is given in units of the Bohr radius, $\rho=R/a$, the energy is noted in units of the Rydberg energy R_∞ for V_{BO} and in units of hR_∞ for the perturbation terms. The arrows indicate the valid ordinate.

$$\rho = R/a \tag{34}$$

gives the internuclear distance in Bohr radii and R_∞ is the Rydberg energy. The radial dependence $\tilde{T}_e(\rho)$ is known numerically and is shown as *C* in Fig. 3. Further, the electronic Coulomb interaction (21) is modified according to (16) so that

$$\delta V_{en} = h\frac{e^2}{4\pi\epsilon_0}\sum_{i=1}^{2}\frac{(x_1 - x_{(i)1})^2 - (x_2 - x_{(i)2})^2}{2|\vec{x} - \vec{x}_{(i)}|^3} \tag{35}$$

describes the corresponding perturbation operator. Integration over the electronic coordinate according to (27) yields

$$\delta V_{en,\mathrm{BO}} = \int d^3x \langle + |x\rangle \delta V_{en} \langle x| + \rangle$$

$$= (hR_\infty)\delta\tilde{V}_{en}(\rho)\cos(2\phi)[1 - \cos(2\theta)]. \tag{36}$$

Again, the radial dependence is known numerically and is shown as *D* in Fig. 3. We next consider the perturbation to the nuclear Coulomb interaction (22) and find according to (16) the following expression for the corresponding perturbation operator:

$$\delta V_{nn} = -h\frac{e^2}{4\pi\epsilon_0}\frac{(x_{(1)1} - x_{(2)1})^2 - (x_{(1)2} - x_{(2)2})^2}{2|\vec{x}_{(1)} - \vec{x}_{(2)}|^3}. \tag{37}$$

Switching to spherical coordinates we obtain

$$\delta V_{nn} = -(hR_\infty)\delta\tilde{V}_{nn}(\rho)\cos(2\phi)[1 - \cos(2\theta)], \tag{38}$$

where $\delta\tilde{V}_{nn}(\rho) = 1/(2\rho)$. Figure 3 points out three important results. First, the modification to the nuclear Coulomb energy (*B*) dominates the perturbation; second, the perturbation is relatively strong near the potential minimum where the radial wave function is largest for low-lying vibrational states. Hence, the rovibrational wave function is as sensitive to the gravitational wave as possible. Finally, the perturbation energy is of the order of $0.1hR_\infty$, i.e., we can expect a shift of the order 30 μHz for a gravitational wave with amplitude $h=10^{-19}$.

We finally must analyze the perturbation to the nuclear kinetic energy (20) which is modified according to (12). The contribution to the relative nuclear motion (23) is given by

$$\delta T_n^m = h\frac{\hbar^2}{2m}(\partial_{R_1}^2 - \partial_{R_2}^2). \tag{39}$$

We switch to spherical coordinates and scale the internuclear distance R to the Bohr radius, $\rho=R/a$. Then the perturbation can be noted as

$$\delta T_n^m = (hR_\infty)\left(\frac{m_e}{m}\right)\delta\tilde{T}_n^m, \tag{40}$$

where

$$\delta\tilde{T}_n^m = \left(\sin\theta\cos\phi\,\partial_\rho + \frac{\cos\theta\cos\phi}{\rho}\partial_\theta - \frac{\sin\phi}{\sin\theta}\partial_\phi\right)^2$$

$$-\left(\sin\theta\sin\phi\partial_\rho + \frac{\cos\theta\sin\phi}{\rho}\partial_\theta + \frac{\cos\phi}{\sin\theta}\partial_\phi\right)^2. \tag{41}$$

Please note that due to the factor (m_e/m) the modification of the nuclear kinetic energy does not contribute significantly to the total perturbation energy.

We can now evaluate the matrix elements of the perturbation operators in the basis $|v\rangle|lm\rangle$ of the unperturbed system. To simplify integration over the radial coordinate we shift the origin of the radial coordinate to the equilibrium internuclear distance R_0, and we normalize the radial coordinate to the vibrational amplitude R_{00}, that describes the typical radial elongation in the vibrational and rotational ground state $|0\rangle|00\rangle$. Hence the new radial coordinate is

$$\epsilon = \frac{\rho - \rho_0}{\rho_{00}}, \tag{42}$$

where $\rho_0=R_0/a$ denotes the equilibrium internuclear distance in units of the Bohr radius and $\rho_{00}=R_{00}/a$ gives the vibrational amplitude in units of the Bohr radius. We also redefine the radial wave function (29) such that

$$\tilde{u}_v(\epsilon) = \sqrt{R_{00}}\,u_v(\epsilon) \tag{43}$$

does not contain any dependence on R_{00} anymore.

Let δA denote any of the perturbation operators describing the electronic kinetic perturbation $\delta T_{e,\mathrm{BO}}$, the electronic Coulomb perturbation $\delta V_{en,\mathrm{BO}}$, or the nuclear Coulomb perturbation δV_{nn}. The quantity $\delta\tilde{A}(\rho)$ may denote the radial-dependent component of these operators according to (33), (36), and (38). The rovibrational matrix elements can then be calculated according to

$$\langle lm|\langle v|\delta A|v'\rangle|l'm'\rangle = \int_\epsilon \int_\theta \int_\phi d\epsilon\, d\theta\, d\phi\, \sin\theta\, \delta A\, Y^*_{lm}(\theta,\phi) \times Y_{l'm'}(\theta,\phi)\, \tilde{u}_v(\epsilon)\, \tilde{u}_{v'}(\epsilon) = (s_\pm hR_\infty) \int_\epsilon d\epsilon\, \delta\tilde{A}(\rho_0+\epsilon\rho_{00})\, \tilde{u}_v(\epsilon) \times \tilde{u}_{v'}(\epsilon) \int_\theta \int_\phi d\theta\, d\phi\, \cos(2\phi)\sin\theta \times [1-\cos(2\theta)] Y^*_{lm}(\theta,\phi)\, Y_{l'm'}(\theta,\phi), \tag{44}$$

where $s_\pm=(+1)$ for $\delta T_{e,\mathrm{BO}}$ and $\delta V_{en,\mathrm{BO}}$ and $s_\pm=(-1)$ for $\delta V_{nn,\mathrm{BO}}$.

The matrix elements for the perturbation to the nuclear kinetic energy cannot be described by (44), because the corresponding operator δT_n^m does neither commute with R nor with θ or ϕ. We find

$$\langle lm|\langle v|\delta T_n^m|v'\rangle|l'm'\rangle = (hR_\infty)\left(\frac{m_e}{m}\right) \int_\epsilon \int_\theta \int_\phi d\epsilon\, d\theta\, d\phi\, \sin\theta \times Y^*_{lm}(\theta,\phi)\, \tilde{u}_v(\epsilon) \left(\frac{1}{\rho}\delta\tilde{T}_n^m \rho\right) \tilde{u}_{v'}(\epsilon) \times Y_{l'm'}(\theta,\phi), \tag{45}$$

where we must replace $\rho=\rho_0+\epsilon\rho_{00}$ and $\partial_\rho=1/\rho_{00}\,\partial_\epsilon$ for integration.

VI. CONSTRUCTION OF THE QUANTUM INTERFEROMETER

With (44) and (45) the perturbation matrix elements can now be evaluated and the perturbation operator can be diagonalized to optimize the rovibrational quantum interferometer for maximum sensitivity to gravitational waves (GWs). We refer to the HD^+ molecular ion for this evaluation.

Figure 4 shows the matrix elements of the total perturbation $\delta T_{e,\mathrm{BO}}+\delta V_{en,\mathrm{BO}}+\delta T_n^m+\delta V_{nn}$ for the $v=0$ vibrational subspace. The GW essentially does not couple different vibrational states or states with different rotational quantum number l. Hence, the diagonalization of the perturbation will yield eigenstates with well-defined rotational quantum number. Obviously, it is sufficient to create rotational coherence in order to optimize the quantum interferometer for the detection of GWs. Figure 4 shows that only states $|v\rangle|l,m\rangle$ and $|v\rangle|l,m\pm2\rangle$ are coupled. The selection rule $|\Delta m|=2$ is expected because of the quadrupole nature of GWs. Figure 4 also shows that the size of the matrix elements does not strongly vary with the rotational quantum number. We have further analyzed the dependence on the vibrational quantum number v and did not find a significant variation with v either.

We next diagonalize the total perturbation operator for the $v=0$ vibrational subspace. The corresponding spectrum of eigenvalues is shown in Fig. 5 for rotational quantum numbers $l=0,\ldots,10$. Eigenstates with larger rotational quantum number tend to exhibit larger shifts. However, the rotational subspace for $l=1$ already provides 91% of the maximum shift observed in the $l=10$ subspace. This is relevant for an experimental realization because fewer laser fields are required to implement the $l=1$ eigenstates. A coherent superposition of the two states $|1_+\rangle$ and $|1_-\rangle$ will then define a rotational quantum interferometer that measures the differential phase shift which accumulates between these states over time due to the interaction with a GW.

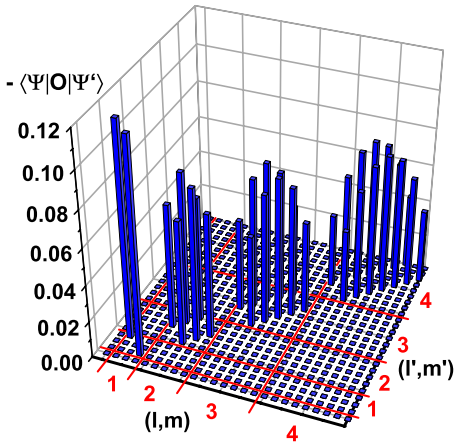

FIG. 4. (Color online) Total perturbation operator $\langle 0|\langle lm|\delta\hat{H}|l'm'\rangle|0\rangle$. The graph shows the matrix elements after multiplication with (-1) in units of hR_∞. The GW couples states with $|\Delta m|=2$. The numbers along the x and y axes (red online) indicate the rotational quantum numbers l and l'.

The most important result, however, is that the size of the differential energy shift is of the order of $0.2h\,R_\infty$. This agrees with our earlier estimate and indicates that a GW with amplitude $h=10^{-19}$ will cause a frequency shift of $\approx 60\ \mu$Hz that is likely to be detectable in 1 s with the next generation atom interferometers.

We next analyze the eigenstates which are optimal for GW detection. For rotational quantum number $l=1$ these are the states labeled $|1_+\rangle$ and $|1_-\rangle$ in Fig. 5. The corresponding

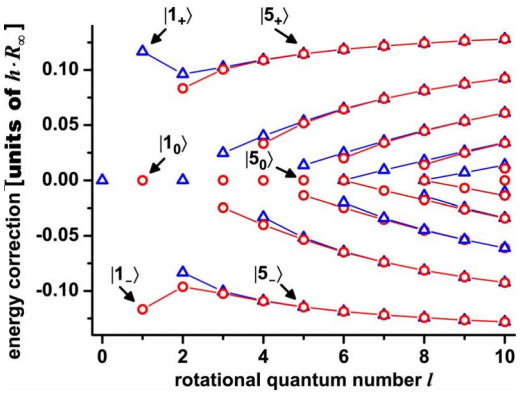

FIG. 5. (Color online) Eigenvalues of the total perturbation operator for the vibrational ground state $v=0$. The ordinate shows the energy shift of the corresponding eigenstates in units of hR_∞ for rotational quantum numbers $l=0,\ldots,10$. The lines are only meant to be a guide for the eye to indicate approximate degeneracy of states. For the definition of the states $|1_+\rangle$, etc., see text.

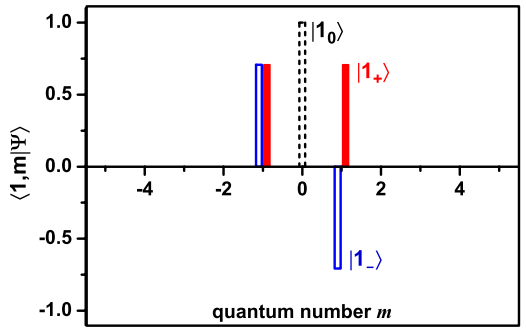

FIG. 6. (Color online) State spectrum of $l=1$ eigenstates of the perturbed molecule. The graph shows the projection $c_{1m}=\langle 1m|\psi\rangle$ of the perturbed eigenstates onto the unperturbed basis. $|1_+\rangle$ and $|1_-\rangle$ denote the two states which experience a differential shift due to the interaction with the GW, see Fig. 5. The state $|1_0\rangle$ is insensitive to GWs.

state spectrum, i.e., the coefficients $c_{1m}=\langle 1m|\psi\rangle$ are the real numbers given in Fig. 6. For $l=1$ the two states corresponding to the two paths of the quantum interferometer are obviously $|1_+\rangle=1/\sqrt{2}(|1,-1\rangle+|1,1\rangle)$ and $|1_-\rangle=1/\sqrt{2}(|1,-1\rangle-|1,1\rangle)$. Only for this specific rotational subspace, the initial state of the quantum interferometer evaluates to an unperturbed eigenstate, namely to $|1_+\rangle+|1_-\rangle\sim|1,-1\rangle$.

As another example we consider the $l=5$ rotational subspace. The optimal eigenstates are $|5_+\rangle$ and $|5_-\rangle$, see Fig. 5. The corresponding state spectrum is shown in Fig. 7. It is obvious that now the initial interferometer state $|5_+\rangle+|5_-\rangle$ no longer corresponds to an unperturbed eigenstate. We recognize further that more molecular states must be coupled coherently for the $l=5$ than for the $l=1$ interferometer which requires larger experimental efforts.

We finally want to check whether the intuitive idea of aligning the internuclear axis of the molecule to perform GW detection is consistent with our findings. To this end we calculate the spherical part of the probability distribution $|\langle\vec{R}|\psi\rangle|^2$ for the eigenstates $|5_+\rangle$, $|5_0\rangle$, and $|5_-\rangle$ and plot them in spherical coordinates in Fig. 8. This visualizes the probability distribution for the orientation of the internuclear axis. The two states $|5_+\rangle$ and $|5_-\rangle$ correspond to an alignment of the internuclear axis in the x-y plane, that is normal to the propagation direction of the GW. The largest energy shift

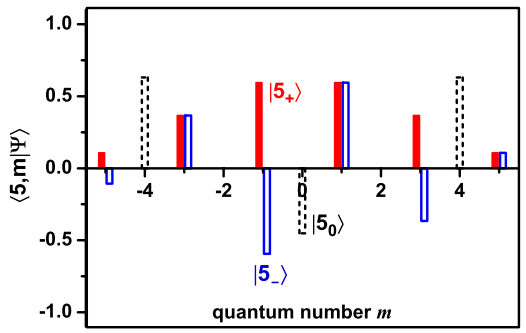

FIG. 7. (Color online) State spectrum of some $l=5$ eigenstates of the perturbed molecule. $|5_+\rangle$ and $|5_-\rangle$ are maximally sensitive to the GW (refer to Fig. 5) whereas $|5_0\rangle$ is insensitive.

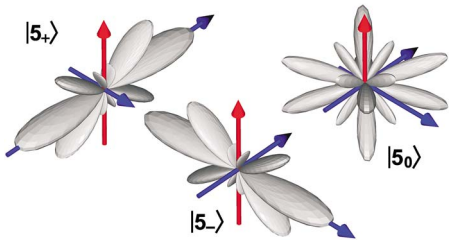

FIG. 8. (Color online) Spherical part of the probability distribution $|\langle\vec{R}|\psi\rangle|^2$ corresponding to the $|5_+\rangle$, $|5_0\rangle$, and $|5_-\rangle$ states, which are optimal for GW detection. The graph visualizes the probability distribution for the orientation of the internuclear molecular axis. The GW is propagating along the vertical direction (red online).

occurs between molecules that are aligned along the x and the y axis, i.e., along the two polarization directions of the GW, as suggest earlier in the qualitative discussion. Consequently, the maximum differential energy shift is observed between states which are aligned along these axes. Figure 8 also shows that states such as $|5_0\rangle$, which are not shifted in energy, do not show any alignment along the x or y direction. We conclude that our findings are in perfect agreement with our intuitive understanding.

Various molecular level schemes exist that could provide GW detection. All of these have in common the notion that states with $|\Delta m|=2$ must be coupled, which can be achieved by means of two-photon Raman transitions. Because the HD^+ molecule provides a vibrational transition between $v=0$ and $v=4$ in the 1400 nm wavelength range, lasers may be used to implement and control the quantum interferometer. The lower-lying vibrational and rotational states are preferred for the implementation of rovibrational quantum interferometers because they provide the longest (coherence) lifetimes. For example, the typical lifetime of the low-lying rotational states within the HD^+ vibrational (and electronic) ground state is well above 1 s [31].

The most simple molecular level scheme suited for GW detection has already been introduced and is depicted as graph (a) in Fig. 9. The most straightforward detector implementation for this scheme consists of only three steps, the preparation step, the actual measurement phase, and the read out step. In the first step the molecules will be prepared in

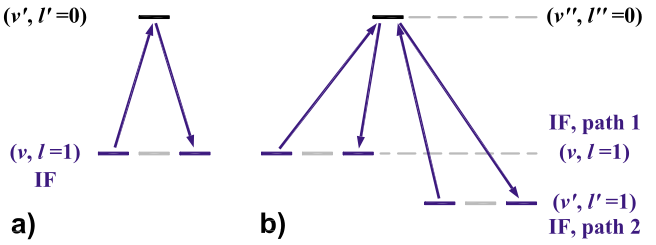

FIG. 9. (Color online) Two molecular level schemes suitable for the implementation of a rotational quantum interferometer that could be used for GW detection. In scheme (a) the same quantum states and optical fields are used to implement both paths of the interferometer. A more detailed control of the implementation is provided by scheme (b) where different quantum states and optical fields are used for the different paths.

the initial interferometer state, say the $|1,+1\rangle$ state, which is a coherent superposition of the two states $|1_+\rangle$ and $|1_-\rangle$ that correspond to the two paths of the interferometer, see Figs. 5 and 6. The preparation step is followed by the measurement phase, in which the two quantum states $|1_+\rangle$ and $|1_-\rangle$ evolve freely in time, however, for no longer than one-half of a GW period. Due to the interaction with the GW a quantum phase shift will accumulate between the two states $|1_+\rangle$ and $|1_-\rangle$. In the final step, these states interfere and are then projected onto the detection state, say the $|1,-1\rangle$ state, by the final laser pulse.

The number of molecules projected onto the detection state carries the information about the differential quantum phase shift between the two interferometer paths. If no phase shift has accumulated, then perfectly destructive interference between the $|1,-1\rangle$ components of the two interferometer states $|1_+\rangle$ and $|1_-\rangle$ implicates that no molecules are detected. In contrast, a nonvanishing phase shift partially prevents the destructive interference of the $|1,-1\rangle$ components so that some molecules are detected.

Scheme (a) of Fig. 9 uses the same quantum states to implement and control both paths of the quantum interferometer. Any laser pulse will therefore unavoidably address both of these paths simultaneously. While this may be desirable for coherent swapping of the two interferometer paths after one-half of a GW period, it prohibits an individual control of the two paths. An individual control, however, may provide means to analyze and compensate systematic effects.

A scheme which provides a more detailed control over the interferometer is shown as graph (b) in Fig. 9. Here, the two quantum states corresponding to the two interferometer paths belong to different vibrational states with quantum numbers v and v'. This provides separate control over the two interferometer paths: The relative phase between the two fields that couple $|v\rangle|1,+1\rangle$ and $|v\rangle|1,-1\rangle$ to $|v''\rangle|0,0\rangle$ defines the quantum state which corresponds to the interferometer path 1. This applies accordingly to interferometer path 2. The relative phase between the two interferometer paths is then controlled by the relative phase between the two "bichromatic" fields. Hence, this scheme guarantees control over the complete set of phases that define the quantum interferometer.

Schemes for the implementation of interferometers that are based on larger rotational quantum numbers are not as obvious. Here, a more detailed analysis is necessary, mainly because the "bichromatic" fields typically couple many more than just the required magnetic sublevels.

VII. OTHER GRAVITATIONAL WAVE DETECTORS

The result of the preceding discussion permits a comparison of rotational molecular quantum interferometric GW detectors to "classical" detectors, i.e., to laser interferometric [7] and bar-type [8] detectors. We finally also address atom interferometric detectors [18].

Let us first recall the unique features of quantum physical sensors. Quantum objects are perfect probes for any kind of ultrahigh sensitivity measurement. First, perfectly identical copies of sensors exist, which, for example, is one of the reasons for defining the unit of time by atomic clocks. Unlike quantum probes macroscopic sensors will never be identical. Hence, they cannot be replaced exactly, if necessary, and it is impossible to have identical sensors at different locations.

Second, the internal structure of real macroscopic objects is so complex that statistical concepts must be used to describe their properties. As an example we may refer to the description of the thermal motion of the test masses used in GW detectors. This description again relies on simplifying assumptions, for example, regarding the crystalline structure or the macroscopic shape of these bodies. The application of statistical concepts also reflects the fact that the interaction between the macroscopic object and its environment is too complex to be described at the atomic scale. In contrast, the internal structure of simple molecules like HD^+ is understood very well. Consequently, the interaction between these quantum sensors and the environment can be controlled very accurately, for example, by shielding or controlling electromagnetic fields. Furthermore, advanced quantum optical methods provide quantum state preparation as one of the indispensable ingredients to quantum interferometry, so that the concept of temperature can be banned from the experiment.

Third, quantum objects are typically localized very well. Again, this is an important advantage over macroscopic objects because it simplifies the description and control of the interaction with the environment.

The most important difference between classical and quantum probes, however, is based on the quantum physical nature of the microscopic probes: First, quantum interferometers provide a phase-sensitive measurement of an energy (frequency) difference which is one of the two reasons for the ultrahigh sensitivity they achieve. Second, quantum interference allows the implementation of several identical copies of a sensor simultaneously and within a single quantum object in a (quantum) phase coherent manner: To realize a molecular quantum interferometric GW detector a single molecule is simultaneously aligned along two orthogonal directions, and the quantum phase difference between the corresponding quantum states is detected. The simultaneous implementation of several sensors within one quantum object is the unique feature, which provides almost perfect rejection of the common mode phase evolution, and of many systematic effects and noise.

Quantum physics also provides the means for quantum phase coherent manipulation of a probe. Coherent manipulation can be applied to overcome the storage time limit of GW detectors. To this end a laser pulse must be applied after one-half of a GW period, that transfers the interferometer state $|1_+\rangle$ into $|1_-\rangle$ and vice versa, if the $l=1$ interferometer of Fig. 9 is considered. Laser interferometric detectors require additional experimental efforts known as signal recycling [32] to overcome this limitation. Further, the direction sensitivity of large scale laser interferometric detectors is not user definable but is only modified by the motion of the earth. In a quantum interferometric GW detector the orientation of the detector can be modified within milliseconds by appropriately setting the phase and amplitude of the laser fields that control the interferometer. The same applies to the polarization sensitivity or to the spectral sensitivity of the GW detector.

We finally address atomic quantum interferometric GW detectors (see [18] and references therein). Similar to molecular quantum GW detectors these benefit at least partially from the quantum physical nature of the probe. However, they are conceptually similar to laser interferometric GW detectors: Matter wave packets are split spatially by optical pulses so that (in an appropriate frame of reference) the subpackets propagate freely along two orthogonal directions. After some time of free propagation, additional laser pulses are applied which redirect the subpackets in analogy to the mirrors which reflect light in laser interferometers. Eventually, the subpackets overlap spatially and (after a final laser pulse) can interfere. The basic idea here is to replace optical waves by matter waves. However, the concept relies on applying the photon recoil to spatially extend the atom interferometer to macroscopic dimensions, so that some of the problems related to classical detectors enter this scheme. Further, light pulses determine the propagation paths of the subpackets. Because the phase of the optical fields is read into the quantum system, phase noise imprinted on the optical fields by seismic and acoustic interference will limit the sensitivity of this type of detectors. This is specifically important as only large scale (10–100 m) [18] interferometers will provide sufficient sensitivity. It is therefore to be expected that the sensitivity of these atom interferometric detectors will typically be comparable to the sensitivity of laser interferometric detectors.

Molecular quantum interferometric GW detectors differ significantly from atom interferometric detectors with respect to this point. They make use of the fact that the GW modifies the internal structure of the sensor, and hence a spatial extension of the molecular wave packet is not required. This circumvents the necessity to define macroscopic spatial extension for an interferometer by optical pulses and therefore eliminates the related problems arising from the spatial variation of phase errors of optical fields. Because the molecular quantum interferometric detector is strongly localized and spatial separation of the wave packet is not required, phase errors of the optical fields will mostly add in common mode and hence will be cancelled out by the differential phase measurement underlying the quantum interferometric principle. The elimination of the external degree of freedom, i.e., of the center-of-mass motion, is a key feature of the molecular quantum interferometric GW detector.

VIII. CONCLUSION

In this paper we presented a type of quantum sensor that may provide tests of fundamental physics with ultrahigh sensitivity. It is based on quantum interferometry, the most sensitive and accurate measurement principle in laboratory-based science.

We generalized the existing concept underlying atom interferometry in a twofold way. First, the basic ideas of atom interferometry were transferred to the internal, i.e., rotational and vibrational states of molecules. Second, we showed that quantum interferometers can be tailor-made to match the specific requirements of a given measurement task. This is achieved by constructing a quantum interferometer from a coherent superposition of typically two states, which themselves are appropriate coherent superpositions of eigenstates of the (unperturbed) quantum system. The novelty here lies in recognizing that the quantum states corresponding to the two paths of the quantum interferometer can be optimized for maximum sensitivity if a specific measurement task is considered.

We further pointed out that atom interferometers can provide a lever arm that boosts their sensitivity beyond what can be achieved with regular laser spectroscopy: Next generation atom interferometers will be able to detect relative frequency shifts of optical transitions at the level of 1 part in 10^{19} in 1 s.

As an application we discussed the detection of gravitational waves with a molecular rovibrational quantum interferometer. The basic idea is to create coherent superpositions of rotational molecular states which correspond to an alignment of the internuclear axis along one of the two polarization directions of the gravitational wave. The two quantum states which correspond to an alignment along these two axes then define the two paths of a quantum interferometer: The interaction with the GW will introduce a quantum phase shift between these states which can then be read out by means of quantum interferometric methods that are well established in atom interferometry. As an example we referred to the HD^+ molecule. We showed that the differential energy shift between two appropriately prepared rovibrational quantum states is of the order of $h0.2R_\infty$, which corresponds to 60 μHz for a strain amplitude of $h=10^{-19}$. Current atom interferometers resolve shifts at the level of 100 μHz, and the next generation interferometers will resolve shifts of 20 μHz in 1 s. This demonstrates the potential that molecular quantum interferometry bears for precision measurements.

We showed that molecular quantum interferometers should be considered for GW detection specifically because of their quantum physical nature. The latter provides a number of tricks that cannot be played with classical devices. We pointed out that, for example, light pulses could swap the two "arms" of a molecular quantum interferometer to overcome the storage time limit. Further, the orientational, polarizational, and spectral sensitivity of molecular quantum GW detectors can simply be controlled by the amplitude, the phase, and the timing of the laser pulses and can be modified at will within milliseconds.

We believe that molecular quantum interferometry holds promise for becoming an important tool for ultrahigh sensitivity quantum metrology.

ACKNOWLEDGMENTS

C.L. would like to thank the German Aerospace Center DLR for financial support. DLR amd D.L. the German Research Foundation and the Centre for Quantum Engineering and Space-Time Research QUEST for financial support.

[1] S. A. Diddams, D. J. Jones, J. Ye, S. T. Cundiff, J. L. Hall, J. K. Ranka, R. S. Windeler, R. Holzwarth, T. Udem, and T. W. Hänsch, Phys. Rev. Lett. **84**, 5102 (2000); S. T. Cundiff and J. Ye, Rev. Mod. Phys. **75**, 325 (2003).

[2] J. Doyle, B. Friedrich, R. V. Krems, and F. Masnou-Seeuws, Eur. Phys. J. D **31**, 149 (2004); T. Bergeman *et al.*, J. Phys. B **39**, S813 (2006).

[3] D. DeMille, Phys. Rev. Lett. **88**, 067901 (2002).

[4] T. Brixner and G. Gerber, ChemPhysChem **4**, 418 (2003); M. S. Elioff, J. J. Valentini, and D. W. Chandler, Science **302**, 1940 (2003).

[5] H. Müller, C. Braxmaier, S. Herrmann, A. Peters, and C. Lämmerzahl, Phys. Rev. D **67**, 056006 (2003).

[6] G. Amelino-Camelia, C. Lämmerzahl, A. Macias, and H. Müller, "The search for quantum gravity signals," in *Gravitation and Cosmology*, edited by A. Macias, C. Lämmerzahl, and D. Nunez, AIP Conference Proceedings 758 (AIP, Melville, New York, 2005), p. 30; D. Mattingly, Living Rev. Relativ. **8**, 5 (2005); D. Mattingly, http://www.livingreviews.org/lrr-2005-5

[7] P. R. Saulson, *Fundamental of Interferometric GW Detectors* (World Scientific, Singapore, 1994); S. Anza *et al.*, Class. Quantum Grav. **22**, S125 (2005); B. J. Owen, *ibid.* **23**, S1 (2006), and references therein.

[8] V. Fafone, Class. Quantum Grav. **21**, S377 (2004), and references therein.

[9] Ch. Lisdat, M. Frank, H. Knöckel, M.-L. Almazor, and E. Tiemann, Eur. Phys. J. D **12**, 235 (2000).

[10] J. J. Hudson, B. E. Sauer, M. R. Tarbutt, and E. A. Hinds, Phys. Rev. Lett. **89**, 023003 (2002).

[11] K. Ohmori, Y. Sato, E. E. Nikitin, and S. A. Rice, Phys. Rev. Lett. **91**, 243003 (2003).

[12] *Atom Interferometry*, edited by P. R. Berman (Academic, New York, 1997); Ch. J. Bordé, Gen. Relativ. Gravit. **36**, 475 (2004).

[13] A. Wicht, J. M. Hensley, E. Sarajlic, and S. Chu, Phys. Scr., T **T102**, 82 (2002).

[14] A. Peters, K. Y. Chung, and S. Chu, Nature (London) **400**, 849 (1999).

[15] J. M. McGuirk, G. T. Foster, J. B. Fixler, M. J. Snadden, and M. A. Kasevich, Phys. Rev. A **65**, 033608 (2002).

[16] T. L. Gustavson, A. Landragin, and M. A. Kasevich, Class. Quantum Grav. **17**, 2385 (2000).

[17] C. Jentsch, T. Müller, E. M. Rasel, and W. Ertmer, Gen. Relativ. Gravit. **36**, 2197 (2004).

[18] G. M. Tino and F. Vetrano, Class. Quantum Grav. **24**, 2167 (2007).

[19] See, for example, the classical experiment: J. L. Hall, C. J. Bordé, and K. Uehara, Phys. Rev. Lett. **37**, 1339 (1976).

[20] For the photon-recoil experiment [13] the two interferometer states are actually based on the $|F,m_F\rangle=|3,0\rangle$ and $|4,0\rangle$ hyperfine states of the electronic ground state of cesium. The interferometer is constructed in such a way that any erroneous detuning of the rf oscillator bridging the 9.2 GHz frequency difference between the hyperfine states cancels the in the measurement. Hence, the energy difference E_{IF} effectively corresponds to $E_{\mathrm{IF}}/h=3752$ Hz as far as the accuracy of the measurement is concerned. In terms of noise, however, the cancellation does not work perfectly and therefore the energy difference between the two quantum states should be considered $E_{\mathrm{IF}}/h=9.2$ GHz.

[21] H. Müller, S.-W. Chiow, Q. Long, and S. Chu, Opt. Lett. **31**, 202 (2006); H. Müller, S.-W. Chiow, Q. Long, Ch. Vo, and S. Chu, Appl. Phys. B: Lasers Opt. **84**, 633 (2006).

[22] H. Müller (private communication).

[23] C. W. Misner, K. S. Thorne, and J. A. Wheeler, *Gravitation* (Freeman, San Francisco, 1973).

[24] A. Brillet, T. Damour, and Ph. Tourrenc, Ann. Phys. **10**, 201 (1985).

[25] T. K. Leen, L. Parker, and L. O. Pimentel, Gen. Relativ. Gravit. **15**, 761 (1983).

[26] C. Kiefer and T. P. Singh, Phys. Rev. D **44**, 1067 (1991).

[27] C. Lämmerzahl, Phys. Lett. A **203**, 12 (1995).

[28] S. Boughn and T. Rothman, Class. Quantum Grav. **23**, 5839 (2006).

[29] G. Herzberg, "I. Spectra of diatomic molecules," *Molecular Spectra and Molecular Structure*, 2nd ed. (van Nostrand Reinhold, New York, 1950); Franz Schwabl, *Quantenmechanik* (Springer, Berlin, Heidelberg, 1988).

[30] *Handbook of Mathematical Functions With Formulas, Graphs, and Mathematical Tables*, edited by M. Abramowitz and I. A. Stegun, Natl. Bur. Stand., Appl. Math. Ser. No. 55 (National Bureau of Standards, Washington, DC, 1972).

[31] Z. Amitay, D. Zajfman, and P. Forck, Phys. Rev. A **50**, 2304 (1994).

[32] H. Grote, A. Fresie, M. Malec, G. Heinzel, B. Willeke, H. Lück, K. Strain, J. Hough, and K. Danzmann, Class. Quantum Grav. **21**, S473 (2004).